Advances in Nano Research, *Vol. 10, No. 2 (2021) 101-114*
DOI: https://doi.org/10.12989/anr.2021.10.2.101

In-plane varying bending force effects on wave dispersion characteristics of single-layered graphene sheets

Yan Cao[1], Abdellatif Selmi[2,3], Rasoul Tohfenamarvar[4], Yousef Zandi[4], Ehsan Kasehchi[5] and Hamid Assilzahed*[6]

[1]*School of Mechatronic Engineering, Xi'an Technological University, Xi'an, 710021 China*
[2]*Department of Civil Engineering, College of Engineering, Prince Sattam Bin Abdulaziz University, Al-Kharj 11942, Saudi Arabia*
[3]*Ecole Nationale d'Ingénieurs deTunis (ENIT), Civil Engineering Laboratory, B.P. 37, Le belvédère1002, Tunis, Tunisia*
[4]*Department of Civil Engineering, Tabriz Branch, Islamic Azad University, Tabriz, Iran*
[5]*Department of Civil Engineering, Roudehen Branch, Islamic Azad University, Roudehen, Iran*
[6]*Institute of Research and Development, Duy Tan University, Da Nang 550000, Vietnam*

(*Received July 2, 2019, Revised September 30, 2020, Accepted October 15, 2020*)

Abstract. An analytical investigation has been performed on the mechanical performance of waves propagated in a Single-Layered Graphene Sheet (SLGS) when an In-plane Varying Bending (IVB) load is interacted. It has been supposed that the Graphene Sheet (GS) is located on an elastic medium. Employing a two-parameter elastic foundation, the effects of elastic substrate on the GS behavior are modeled. Besides, the kinematic equations are derived by the means of a trigonometric two-variable refined plate theory. Moreover, in order to indicate the size-dependency of the SLGS, a Nonlocal Strain Gradient Theory (NSGT) was considered. The nonlocal governing differential equations are achieved in the framework of Hamilton's Principle (HP). Also, an analytical approach was used to detect the unknowns of the final eigenvalue equation. Finally, the effects of each parameters using some dispersion charts were determined.

Keywords: wave propagation; single-layered graphene sheet (SLGS); nonlocal strain gradient theory (NSGT); Winkler-Pasternak foundation; varying bending force

1. Introduction

In recent years, great motivation has been observed in science society about utilizing nano-sized elements to analyze the mechanical behaviors of structures. Since employing nanoscale beams and plates are popular among many scholars, it is very important to obtain sufficient information about the size-dependent (SD) behaviors of these tiny elements (Shariati *et al*. 2020a, b, Toghroli *et al*. 2020). Therefore, in order to explain the small-scale influences while studying the mechanical characteristics of nanodevices, the nonlocal continuum theories are developed (Alaskar *et al*. 2020a, b, Huang *et al*. 2020a, Luo *et al*. 2020). The first Nonlocal Theory (NT) which was called Nonlocal Elasticity Theory (NET), which relates the stress state in a desired point to the strain of all other adjacent points in addition to the strain of that particular point (Alaskar *et al*. 2020c, Alyousef *et al*. 2020, Cao *et al*. 2020a, d). Many authors have used this theory. Hence, recent studies using NET to investigate the mechanical responses of nanobeams or plates are reviewed. The buckling, bending and Free Vibration Responses (FVR) of nanobeams examined (Aydogdu 2009). The forced vibrations of Functionally Graded (FG) microbeams considering the effect of cracks evaluated (Akbaş 2018). The buckling response of magneto-electro-elastic nanobeam and FG heterogeneous piezoelectric nanobeams was probed (Arani *et al*. 2016). A new refined nonlocal beam theory which considers the stretching effect in nanobeam was developed (Kheroubi *et al*. 2016). The critical buckling temperature of single-walled boron nitride nanotubes through their formulation developed on the basis of a novel nonlocal beam model was proposed as well. The Wave Dispersion (WD) characteristics of nanoplates using NET were evaluated (Wang *et al*. 2010). The FVR of orthotropic arbitrary straight-sided quadrilateral nanoplates was indicated by Malekzadeh *et al*. (2011). Narendar and Gopalakrishnan (2012) studied the effect of temperature on the WD properties of SD plates. Besides, the influence of surface on Wave Propagation (WP) behaviors of a nanoplate was described by Narendar and Gopalakrishnan (2012). The vibrational properties of nanobeams employing Finite Element Method (FEM) and Euler-Bernoulli beam theory was explained by Eltaher *et al*. (2013). Ghadiri and Shafiei (2016) employed Differential Quadrature Method (DQM) for bending vibration on analysis of nanobeams. The frequency response study of double walled Carbon Nanotubes (CNs) embedded in an elastic medium with initial imperfection was carried out. Further, assessment of the porosity and preloading effect on the frequencies of rotating FG nanobeams was studied. Ebrahimi and Barati (2016a, b, d, e, 2017a, b, c, 2018), Ebrahimi *et al*. (2016a,

*Corresponding author, Ph.D.,
E-mail: hamidassilzadeh@duytan.edu.vn

ISSN: 2287-237X (Print), 2287-2388 (Online)

b, c, d), Ebrahimi and Dabbagh (2017) applied the NET to examined the mechanical responses of SD beams and plates under different external forces. A new nonlocal Higher Order Shear Deformation (HOSD) theory to demonstrate the stability properties of SLGSs was used. Over the years, scientists have discovered that the NET is not powerful enough to thoroughly study the small structures behavior (Lam *et al*. 2003). This means that the only stiffness-softening behavior is considered and stiffness-hardening effect of nanostructures has been overlooked in NET. Therefore, a new Nonlocal Theory (NT), called NSGT was developed to eliminate the mentioned shortage (Lim *et al*. 2015). For highlighting the size effects, a NSGT was suggested by Li and Hu (2015), while analyzing the buckling responses of nanobeams. Farajpour *et al*. (2016) studied the thermo-mechanical buckling properties of orthotropic nanoplates using NSG. The forced response study of metal foam porous nanoplates was performed based on NSGT. The WD properties of nanobeams and nanoplates were studied employing NSGT by Ebrahimi and Barati (2016d, e). More recently, it was demonstrated that the nonlocal differential and integral elasticity-based models may be not equivalent to each other (Zhu and Li 2017c). Zhu and Li (2017b) formulated the longitudinal dynamic problem of SD monolayer graphene nano-rod using integral form of NSGT. Zhu and Li (2017a) extended their evaluation to develop a SD integral elasticity model for small-scaled CNT rods in tension based on NSGT. The SD effects across the thickness direction of beams and plates are often assumed to be neglected for the sake of simplification. However, few prominent literatures have demonstrated that it is crucial to consider the SD effects across the thickness of nanostructures (Li *et al*. 2018, Tang *et al*. 2019). On the contrary, many carbon-based materials can be determined which leads to making some distortions in GSs (Ebrahimi and Salari 2015). Moreover, compared to other small structures which have been composed of various materials such as elastic potential (Lee *et al*. 2008) and larger thermal conductivity (Seol *et al*. 2010), GSs have some advantages. Based on mentioned explanations, obtaining accurate findings about the mechanical responses of these types of nanostructures is an essential issue. Hence, Murmu and Pradhan (2009) examined the dynamic responses of embedded SLGSs using Eringen's NT. Also, investigation on SD buckling behaviors of SLGSs was conducted by Pradhan and Murmu (2010). Besides, Pradhan and Kumar (2011) employed DQM to reveal the authenticity of this solution method in addressing vibration problems of orthotropic SLGSs. An atomistic FE based model was introduced for vibration and axial buckling assessment of SLGSs (Rouhi and Ansari 2012). Arash *et al*. (2012) used NET to scrutinize the SD mechanical characteristics of propagating waves in GSs. Murmu *et al*. (2013) employed NET to examine the transverse vibrational behaviors of a magnetically influenced SLGS. Moreover, magneto-mechanical vibration and stability evaluation of SLGSs rested on Viscoelastic Foundation (VF) was the subject of another study conducted by Zenkour (2016) surveyed the transient vibration problem of a SLGS rested on a VF. Further, Zenkour (2016) investigated the stability response of GS resting on elastic foundation using nonlocal first order theory. Ebrahimi and Shafiei (2017) evaluated the vibrational responses of SLGSs rested on Winkler-Pasternak foundation to study the effect of initial shear stress (Alabduljabbar *et al*. 2020, Cao *et al*. 2020b, c, Liu *et al*. 2020b). Recently, a NSGT based theory was introduced by Xiao *et al*. (2017) to examine the WP behaviors of viscoelastic Mono-Layered Graphene Sheets (MLGSs). Phung-Van *et al*. (2019b) briefly discussed the porosity-dependent nonlinear transient responses of FG nanoplates employing isogeometric assessment. An isogeometric method of static and free vibration assessments for porous FG nanoplates analyzed by Phung-Van *et al*. (2019a). Thai *et al*. (2020) investigated the SD quasi-3D isogeometric model for FG graphene platelet-reinforced composite microplates based on the modified couple stress theory. Thai *et al*. (2019) scrutinized SD free vibration analysis of multilayer functionally graded GPLRC microplates based on modified strain gradient theory. An isogeometric approach for SD geometrically nonlinear transient analysis of FG nanoplates deliberated by Phung-Van *et al*. (2017a). Phung-Van *et al*. (2017b) dissected SD isogeometric analysis of FG carbon nanotube-reinforced composite nanoplates. Graphene-based materials and their composites have been extensively investigated in recent years (Zuo *et al*. 2015, 2017, Gao *et al*. 2018a, Cai *et al*. 2020b, Liu *et al*. 2020c, Song *et al*. 2020). Liu *et al*. (2020a) evaluated the development of applying graphene-based nanomaterials in enhancing the properties of cementitious material. With advances in nanotechnology, several studies have been performed on nanostructures (Chen *et al*. 2020, Huang *et al*. 2020b, Shi *et al*. 2020a, Wang *et al*. 2020, Xu *et al*. 2020, Yan *et al*. 2020, Zhu *et al*. 2020). It is obvious that the exceptional properties of these valuable materials have attracted the scholars' attention to use them in various engineering and medical applications (Chen *et al*. 2018, Guo *et al*. 2019, Cai *et al*. 2020a, c, Shi *et al*. 2020b, Zuo *et al*. 2020a). Artificial Intelligence (AI) algorithms can be used to predict the different characteristics of nanoplates under different loading conditions instead of other classical methods (Mohammadhassani *et al*. 2013, 2014, Toghroli *et al*. 2014, 2018, Safa *et al*. 2016, 2020, Gao *et al*. 2018b, Sadeghipour Chahnasir *et al*. 2018, Sedghi *et al*. 2018, Katebi *et al*. 2019, Mansouri *et al*. 2019, Milovancevic *et al*. 2019, Qiu *et al*. 2019, Suhatril *et al*. 2019, Trung *et al*. 2019, Qi 2020, Qian *et al*. 2020a, b, Zhao *et al*. 2020a, Zuo *et al*. 2020b). Moreover, the finite element method is one of the numerical approaches which can be employed in the analysis of nanostructures (Zuo *et al*. 2013, Gao and Zhang 2019, Zhao *et al*. 2019, 2020b, Guo *et al*. 2020, Hu *et al*. 2020, Zhang *et al*. 2020a, b). As it was explained in the literature, results show that limited studies have been performed on WP of SLGs. Meanwhile, to the best of authors' knowledge, no research has been conducted on the WP analysis of SLGSs under an in-plane linearly varying force. Therefore, it is essential to survey this problem for the first time through NSGT. The GS is assumed to be rested on an elastic substrate including a linear constant (Winkler coefficient) and a nonlinear constant (Pasternak coefficient). The effects of shear deformation are covered

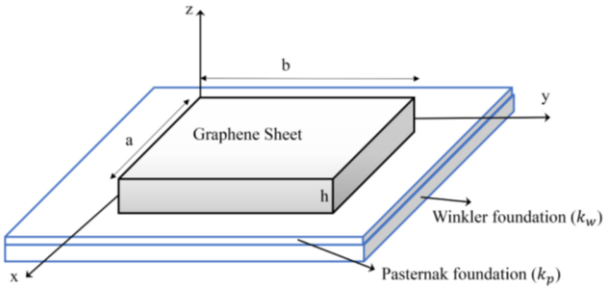

Fig. 1 Geometry of a SLGS rested on Winkler-Pasternak foundation

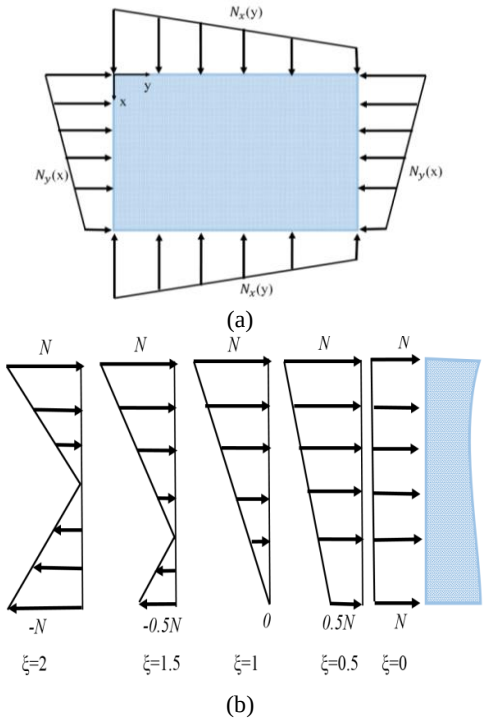

Fig. 2 (a) General form of GSs under IVB forces (b) Various kinds of IVB forces

utilizing a two-variable HOSD plate theory. Besides, in order to consider the small scale influences, two nonlocal and length scale parameters are presented. Once the nonlocal differential equations are completely obtained, they will be solved analytically using an exponential function. At the end of the study, the quality of each parameter's effect is indicated by the means of some diagrams.

2. Theory and formulation

2.1 Kinematic relations

This section explains the kinematic behaviors of GSs. Fig. 1 indicates the schematic of an embedded SLGS. A refined higher-order plate theory was employed to determine the effects of shear deformation. Therefore, the displacement fields can be formulated as Ebrahimi and Barati (2016c)

$$U(x,y,z) = -z\frac{\partial w_b}{\partial x} - f(z)\frac{\partial w_s}{\partial x} \tag{1}$$

$$V(x,y,z) = -z\frac{\partial w_b}{\partial y} - f(z)\frac{\partial w_s}{\partial y} \tag{2}$$

$$W(x,y,z) = w_b(x,y) + w_s(x,y) \tag{3}$$

where w_s and w_b are shear and bending deflections in the thickness direction, respectively. Besides, $f(z)$ is a shape function that determines shear stress and shear strain. In the current theory, a trigonometric function is employed as

$$f(z) = z - \frac{h}{\pi}\sin\left(\frac{\pi z}{h}\right) \tag{4}$$

where h shows the thickness of plate. So, the nonzero strains can be presented as follows

$$\begin{Bmatrix}\varepsilon_x\\ \varepsilon_y\\ \gamma_{xy}\end{Bmatrix} = z\begin{Bmatrix}-\frac{\partial^2 w_b}{\partial x^2}\\ -\frac{\partial^2 w_b}{\partial y^2}\\ -2\frac{\partial^2 w_b}{\partial x\partial y}\end{Bmatrix} + f(z)\begin{Bmatrix}-\frac{\partial^2 w_s}{\partial x^2}\\ -\frac{\partial^2 w_s}{\partial y^2}\\ -2\frac{\partial^2 w_s}{\partial x\partial y}\end{Bmatrix}$$
$$\begin{Bmatrix}\gamma_{yz}\\ \gamma_{xz}\end{Bmatrix} = g(z)\begin{Bmatrix}\frac{\partial w_s}{\partial y}\\ \frac{\partial w_s}{\partial x}\end{Bmatrix} \tag{5}$$

In Eq. (5), $g(z)$ can be stated as

$$g(z) = 1 - \frac{df(z)}{dz} \tag{6}$$

Also, the HP can be described as

$$\int_0^t \delta(U - T + V)\mathrm{d}t = 0 \tag{7}$$

where U, T and V are strain energy, kinetic energy and work done by external loads, respectively. The strain energy variation can be obtained through

$$\delta U = \int_V \sigma_{ij}\delta\varepsilon_{ij}dV$$
$$= \int_V \left(\sigma_x\delta\varepsilon_x + \sigma_y\delta\varepsilon_y + \sigma_{xy}\delta\gamma_{xy} + \sigma_{yz}\delta\gamma_{yz} + \sigma_{xz}\delta\gamma_{xz}\right)\mathrm{d}V \tag{8}$$

Substituting Eq. (5) in Eq. (8) shows

$$\delta U = \int_0^a\int_0^b \begin{pmatrix} -M_x^b\frac{\partial^2\delta w_b}{\partial x^2} - M_x^s\frac{\partial^2\delta w_s}{\partial x^2} - M_y^b\frac{\partial^2\delta w_b}{\partial y^2} - M_y^s\frac{\partial^2\delta w_s}{\partial y^2} - \\ 2M_{xy}^b\frac{\partial^2\delta w_b}{\partial x\partial y} - 2M_{xy}^s\frac{\partial^2\delta w_s}{\partial x\partial y} + Q_{xz}\frac{\partial\delta w_s}{\partial x} + Q_{yz}\frac{\partial\delta w_s}{\partial y} \end{pmatrix}\mathrm{d}y\mathrm{d}x \tag{9}$$

The unknown parameters in above equation can be explained as follows

$$\begin{aligned}&\left(M_i^b, M_i^s\right)=\int_{-\frac{h}{2}}^{\frac{h}{2}}(z,f)\sigma_i dz\\&i=(x,y,xy)\\&Q_i=\int_{-\frac{h}{2}}^{\frac{h}{2}}g\sigma_i dz\\&i=(xz,yz)\end{aligned}\tag{10}$$

In addition, variation of work done by external loads can be indicated as

$$\begin{aligned}&k_p\nabla^2(w_b+w_s)-N_x^0\frac{\partial^2(w_b+w_s)}{\partial x^2}-N_y^0\frac{\partial^2(w_b+w_s)}{\partial y^2}\\&-k_w(w_b+w_s)-I_0\frac{\partial^2(w_b+w_s)}{\partial t^2}+J_2\nabla^2\left(\frac{\partial^2 w_b}{\partial t^2}\right)\\&+K_2\nabla^2\left(\frac{\partial^2 w_s}{\partial t^2}\right)=0\end{aligned}$$

2.2 The nonlocal strain gradient theory (NSGT)

Based on NSGT, the influences of nonlocal elastic stress field in addition to the stain gradient stress field are considered by stress field. Hence, for elastic solids, the theory can be stated as

$$\delta V=\int_0^a\int_0^b\left(\begin{array}{c}N_x^0\frac{\partial(w_b+w_s)}{\partial x}\frac{\partial\delta(w_b+w_s)}{\partial x}+N_y^0\frac{\partial(w_b+w_s)}{\partial y}\frac{\partial\delta(w_b+w_s)}{\partial y}+\\2\delta N_{xy}^0\frac{\partial(w_b+w_s)}{\partial x}\frac{\partial(w_b+w_s)}{\partial y}-k_w\delta(w_b+w_s)+\\k_p\left(\frac{\partial(w_b+w_s)}{\partial x}\frac{\partial\delta(w_b+w_s)}{\partial x}+\frac{\partial(w_b+w_s)}{\partial y}\frac{\partial\delta(w_b+w_s)}{\partial y}\right)\end{array}\right)\mathrm{d}y\mathrm{d}x\tag{11}$$

where N_x^0, N_y^0, N_{xy}^0 are in-plane applied loads; k_w and k_p are Winkler and Pasternak coefficients. GS is considered to be subjected to a varying bending force in x and y directions defined as follows (while N_{xy}^0 = 0)

$$N_x^0=N\left(1-\zeta\frac{y}{b}\right),\qquad N_y^0=\lambda N\left(1-\zeta\frac{x}{a}\right)\tag{12}$$

In above equation, ζ is in-plane bending load factor. Also, λ denotes biaxial load factor. The different types of in-plane linearly varying bending forces are illustrated in Fig. 2. The kinetic energy variation should be presented as

$$\delta K=\int_0^a\int_0^b\left(\begin{array}{c}I_0\left(\frac{\partial(w_b+w_s)}{\partial t}\frac{\partial\delta(w_b+w_s)}{\partial t}\right)+I_2\left(\frac{\partial w_b}{\partial x\partial t}\frac{\partial\delta w_b}{\partial x\partial t}+\frac{\partial w_b}{\partial y\partial t}\frac{\partial\delta w_b}{\partial y\partial t}\right)\\+K_2\left(\frac{\partial w_s}{\partial x\partial t}\frac{\partial\delta w_s}{\partial x\partial t}+\frac{\partial w_s}{\partial y\partial t}\frac{\partial\delta w_s}{\partial y\partial t}\right)+\\J_2\left(\frac{\partial w_b}{\partial x\partial t}\frac{\partial\delta w_s}{\partial x\partial t}+\frac{\partial w_s}{\partial x\partial t}\frac{\partial\delta w_b}{\partial x\partial t}+\frac{\partial w_b}{\partial y\partial t}\frac{\partial\delta w_s}{\partial y\partial t}+\frac{\partial w_s}{\partial y\partial t}\frac{\partial\delta w_b}{\partial y\partial t}\right)\end{array}\right)\mathrm{d}y\mathrm{d}x\tag{13}$$

in which

$$(I_0,I_2,J_2,K_2)=\int_{-\frac{h}{2}}^{\frac{h}{2}}(1,z^2,zf,f^2)\rho dz\tag{14}$$

Inserting Eqs. (9), (11) and (13) in Eq. (7) and setting the coefficients of δw_b and δw_s to zero, the Euler-Lagrange equations of GSs can be rewritten as

$$\begin{aligned}&\frac{\partial^2 M_x^b}{\partial x^2}+2\frac{\partial^2 M_{xy}^b}{\partial x\partial y}+\frac{\partial^2 M_y^b}{\partial y^2}+k_p\nabla^2(w_b+w_s)\\&-k_w(w_b+w_s)-N_x^0\frac{\partial^2(w_b+w_s)}{\partial x^2}-N_y^0\frac{\partial^2(w_b+w_s)}{\partial y^2}\\&-I_0\frac{\partial^2(w_b+w_s)}{\partial t^2}+I_2\nabla^2\left(\frac{\partial^2 w_b}{\partial t^2}\right)+J_2\nabla^2\left(\frac{\partial^2 w_s}{\partial t^2}\right)=0\end{aligned}\tag{15}$$

$$\frac{\partial^2 M_x^s}{\partial x^2}+2\frac{\partial^2 M_{xy}^s}{\partial x\partial y}+\frac{\partial^2 M_y^s}{\partial y^2}+\frac{\partial Q_{xz}}{\partial x}+\frac{\partial Q_{yz}}{\partial y}+\tag{16}$$

Based on NSGT, the influences of nonlocal elastic stress field in addition to the stain gradient stress field are considered by stress field. Hence, for elastic solids, the theory can be stated as

$$\sigma_{ij}=\sigma_{ij}^{(0)}-\frac{d\sigma_{ij}^{(1)}}{dx}\tag{17}$$

In Eq. (17), the stresses $\sigma_{xx}^{(0)}$ (classical stress) and $\sigma_{xx}^{(1)}$ (higher-order stress) are corresponding to strain ε_{xx} and strain gradient $\varepsilon_{xx,x}$, respectively as relations (equations) below

$$\begin{cases}\sigma_{ij}^{(0)}=\int_0^L C_{ijkl}\,\alpha_0(x,x',e_0a)\varepsilon'_{kl}(x')dx'\\\sigma_{ij}^{(1)}=l^2\int_0^L C_{ijkl}\,\alpha_1(x,x',e_1a)\varepsilon'_{kl,x}(x')dx'\end{cases}\tag{18}$$

where C_{ijkl} is the elastic coefficient; e_0a and e_1a are presented to determine the nonlocality influences. Also, the effects of strain gradient are captured by l. Once the nonlocal kernel functions $\alpha_0(x,x',e_0a)$ and $\alpha_1(x,x',e_1a)$ satisfy the developed conditions, the constitutive relation of NSGT can be obtained as below

$$\begin{aligned}&(1-(e_1a)^2\nabla^2)(1-(e_0a)^2\nabla^2)\sigma_{ij}=\\&C_{ijkl}(1-(e_1a)^2\nabla^2)\varepsilon_{kl}-\\&C_{ijkl}l^2(1-(e_0a)^2\nabla^2)\nabla^2\varepsilon_{kl}\end{aligned}\tag{19}$$

where ∇^2 demonstrate the Laplacian operator. Considering $e_1 = e_0 = e$, the general constitutive relation in Eq. (19) would be

$$(1-(ea)^2\nabla^2)\sigma_{ij} = C_{ijkl}(1-l^2\nabla^2)\varepsilon_{kl} \tag{20}$$

Ultimately, the simplified constitutive equation can be determined through

$$(1-\mu^2\nabla^2)\begin{Bmatrix}\sigma_x\\ \sigma_y\\ \sigma_{xy}\\ \sigma_{yz}\\ \sigma_{xz}\end{Bmatrix} = (1-\eta^2\nabla^2)\times \begin{pmatrix} Q_{11} & Q_{12} & 0 & 0 & 0\\ Q_{12} & Q_{22} & 0 & 0 & 0\\ 0 & 0 & Q_{66} & 0 & 0\\ 0 & 0 & 0 & Q_{44} & 0\\ 0 & 0 & 0 & 0 & Q_{55}\end{pmatrix}\begin{Bmatrix}\varepsilon_x\\ \varepsilon_y\\ \gamma_{xy}\\ \gamma_{yz}\\ \gamma_{xz}\end{Bmatrix} \tag{21}$$

In above equation

$$Q_{11} = Q_{22} = \frac{E}{1-\nu^2}, \qquad Q_{12} = \nu Q_{11}$$
$$Q_{44} = Q_{55} = Q_{66} = \frac{E}{2(1+\nu)} \tag{22}$$

where $\mu = e_0 a$ and $\eta = l$. Substituting Eq. (10) in Eq. (21) gives

$$(1-\mu^2\nabla^2)\begin{Bmatrix}M_x^b\\ M_y^b\\ M_{xy}^b\end{Bmatrix} = (1-\eta^2\nabla^2)\left(\begin{pmatrix} D_{11} & D_{12} & 0\\ D_{12} & D_{22} & 0\\ 0 & 0 & D_{66}\end{pmatrix}\times\begin{Bmatrix} -\frac{\partial^2 w_b}{\partial x^2}\\ -\frac{\partial^2 w_b}{\partial y^2}\\ -2\frac{\partial^2 w_b}{\partial x\partial y}\end{Bmatrix} + \begin{pmatrix} D_{11}^s & D_{12}^s & 0\\ D_{12}^s & D_{22}^s & 0\\ 0 & 0 & D_{66}^s\end{pmatrix}\begin{Bmatrix} -\frac{\partial^2 w_s}{\partial x^2}\\ -\frac{\partial^2 w_s}{\partial y^2}\\ -2\frac{\partial^2 w_s}{\partial x\partial y}\end{Bmatrix}\right) \tag{23}$$

$$(1-\mu^2\nabla^2)\begin{Bmatrix}M_x^s\\ M_y^s\\ M_{xy}^s\end{Bmatrix} = (1-\eta^2\nabla^2)\left(\begin{pmatrix} D_{11}^s & D_{12}^s & 0\\ D_{12}^s & D_{22}^s & 0\\ 0 & 0 & D_{66}^s\end{pmatrix}\times\begin{Bmatrix} -\frac{\partial^2 w_b}{\partial x^2}\\ -\frac{\partial^2 w_b}{\partial y^2}\\ -2\frac{\partial^2 w_b}{\partial x\partial y}\end{Bmatrix} + \begin{pmatrix} H_{11}^s & H_{12}^s & 0\\ H_{12}^s & H_{22}^s & 0\\ 0 & 0 & H_{66}^s\end{pmatrix}\times\begin{Bmatrix} -\frac{\partial^2 w_s}{\partial x^2}\\ -\frac{\partial^2 w_s}{\partial y^2}\\ -2\frac{\partial^2 w_s}{\partial x\partial y}\end{Bmatrix}\right) \tag{24}$$

$$(1-\mu^2\nabla^2)\begin{Bmatrix}Q_x\\ Q_y\end{Bmatrix} = (1-\eta^2\nabla^2)\left(\begin{pmatrix} A_{44}^s & 0\\ 0 & A_{55}^s\end{pmatrix}\begin{Bmatrix}\frac{\partial w_s}{\partial x}\\ \frac{\partial w_s}{\partial y}\end{Bmatrix}\right) \tag{25}$$

In Eqs. (23) to (25), the cross-sectional rigidities can be introduced as

$$\begin{pmatrix} D_{11} & D_{11}^s & H_{11}^s\\ D_{12} & D_{12}^s & H_{12}^s\\ D_{66} & D_{66}^s & H_{66}^s\end{pmatrix} = \int_{-h/2}^{h/2} Q_{11}(z^2 \quad zf \quad f^2)\begin{Bmatrix}1\\ \nu\\ \frac{1-\nu}{2}\end{Bmatrix}dz \tag{26}$$

$$A_{44}^s = A_{55}^s = \int_{-h/2}^{h/2} g^2\frac{E}{2(1+\nu)}dz \tag{27}$$

By substituting Eqs. (23) to (25) in Eqs. (14) and (15), the nonlocal governing equations of SLGSs can be directly derived in terms of displacements as

$$\begin{aligned}&(1-\eta^2\nabla^2)\times\\ &\begin{pmatrix} -D_{11}\frac{\partial^4 w_b}{\partial x^4} - 2(D_{12}+2D_{66})\frac{\partial^4 w_b}{\partial x^2\partial y^2} - D_{22}\frac{\partial^4 w_b}{\partial y^4}\\ -D_{11}^s\frac{\partial^4 w_s}{\partial x^4} - 2(D_{12}^s+2D_{66}^s)\frac{\partial^4 w_s}{\partial x^2\partial y^2} - D_{22}^s\frac{\partial^4 w_s}{\partial y^4}\end{pmatrix}\\ &+(1-\mu^2\nabla^2)\times\\ &\begin{pmatrix} -I_0\frac{\partial^2(w_b+w_s)}{\partial t^2} + I_2\left(\frac{\partial^4 w_b}{\partial x^2\partial t^2}+\frac{\partial^4 w_b}{\partial y^2\partial t^2}\right)\\ +J_2\left(\frac{\partial^4 w_s}{\partial x^2\partial t^2}+\frac{\partial^4 w_s}{\partial y^2\partial t^2}\right) + k_p\left(\frac{\partial^2(w_b+w_s)}{\partial x^2}\right.\\ \left.+\frac{\partial^2(w_b+w_s)}{\partial y^2}\right) - k_w(w_b+w_s)\\ -N_x^0\frac{\partial^2(w_b+w_s)}{\partial x^2} - N_y^0\frac{\partial^2(w_b+w_s)}{\partial y^2}\end{pmatrix} = 0\end{aligned} \tag{28}$$

$$\begin{aligned}&(1-\eta^2\nabla^2)\times\\ &\begin{pmatrix} -D_{11}^s\frac{\partial^4 w_b}{\partial x^4} - 2(D_{12}^s+2D_{66}^s)\frac{\partial^4 w_b}{\partial x^2\partial y^2} - D_{22}^s\frac{\partial^4 w_b}{\partial y^4}\\ -H_{11}^s\frac{\partial^4 w_s}{\partial x^4} - 2(H_{12}^s+2H_{66}^s)\frac{\partial^4 w_s}{\partial x^2\partial y^2} - H_{22}^s\frac{\partial^4 w_s}{\partial y^4}\\ +A_{44}^s\frac{\partial^2 w_s}{\partial x^2} + A_{55}^s\frac{\partial^2 w_s}{\partial y^2}\end{pmatrix}\\ &+(1-\mu^2\nabla^2)\times\\ &\begin{pmatrix} -I_0\frac{\partial^2(w_b+w_s)}{\partial t^2} + J_2\left(\frac{\partial^4 w_b}{\partial x^2\partial t^2}+\frac{\partial^4 w_b}{\partial y^2\partial t^2}\right)\\ +K_2\left(\frac{\partial^4 w_s}{\partial x^2\partial t^2}+\frac{\partial^4 w_s}{\partial y^2\partial t^2}\right) + k_p\left(\frac{\partial^2(w_b+w_s)}{\partial x^2}\right.\\ \left.+\frac{\partial^2(w_b+w_s)}{\partial y^2}\right) - k_w(w_b+w_s)\\ -N_x^0\frac{\partial^2(w_b+w_s)}{\partial x^2} - N_y^0\frac{\partial^2(w_b+w_s)}{\partial y^2}\end{pmatrix} = 0\end{aligned} \tag{29}$$

3. Analytical solution

In this section, the nonlocal governing equations determined in previous part would be solved analytically. The displacement fields are supposed to be exponential and can be introduced through

$$\begin{Bmatrix}w_b(x,y,t)\\ w_s(x,y,t)\end{Bmatrix} = \begin{Bmatrix}W_b\, exp[i(\beta_1 x+\beta_2 y-\omega t)]\\ W_s\, exp[i(\beta_1 x+\beta_2 y-\omega t)]\end{Bmatrix} \tag{30}$$

where W_b and W_s are the unknown coefficients; β_1 and β_2 are the wave numbers of WP along x and y directions respectively, and finally ω is Wave's Angular Frequency (WAF). So, substituting Eq. (30) to Eqs. (28) and (29) leads to

$$([K]_{2\times 2} - \omega^2[M]_{2\times 2})\{\Delta\} = \{0\} \tag{31}$$

Table 1 Comparison of frequency of FG nanoplates for different nonlocal parameters (p = 5)

μ	a/h = 10 Natarajan *et al.* (2012)	Present	a/h = 20 Natarajan *et al.* (2012)	Present
0	0.0441	0.043803	0.0113	0.011255
1	0.0403	0.040051	0.0103	0.010288
2	0.0374	0.037123	0.0096	0.009534
4	0.033	0.032791	0.0085	0.008418

where the corresponding k_{ij} and m_{ij} has been formulated in the appendix. The unknown parameters of Eq. (3) can be written as

$$\{\Delta\} = \{W_b, W_s\}^T \tag{32}$$

In order to attaining the WAF, the determinant of the left hand side of Eq. (32) should be set to zero

$$|[K]_{2\times2} - \omega^2[M]_{2\times2}| = 0 \tag{33}$$

In above equation by setting $\beta_1 = \beta_2 = \beta$ and solving the obtained equation for ω, the WAF of embedded SLGSs can be obtained. If the angular frequency is divided by wave number, the phase velocity can be determined as follows

$$c = \frac{\omega}{\beta} \tag{34}$$

Moreover, by tending wave number to infinity, the escape frequency of GS can be determined

$$\tilde{\omega} = \lim_{\beta\to\infty} \frac{\omega}{2\pi} \tag{35}$$

4. Results

The WP responses of SLGSs are compared once different parameters are assumed to be changed. The thermo-mechanical material properties of GSs are: E = 1 TPa, v = 0.19, ρ = 2300 kg/m^3. Moreover, the thickness is considered to be h = 0.34 nm. Wave frequencies in following figures are determined by dividing WAF to 2π ($f = \frac{\omega}{2\pi}$). Moreover, the validity of reported results is confirmed by comparing the results between this study with those of previous papers as illustrated in Table 1. Fig. 3 indicates the coupled effects of strain gradient parameter and linearly varying bending loads in $-x$ and $-y$ directions on the wave frequency values while μ = 1 nm. Based on these diagrams, it is clear that the stiffness-hardening phenomenon discussed in NSGT can be figured out.

In other words, Fig. 3(a) describes the size-dependency of GSs by the means of the NET, whereas, in Figs. 3(b), (c) and (d), the NSGT is employed. As same as the basic assumptions of the NSGT, wave frequency intensifies once the length scale parameter is added. Besides, it can be concluded that the greater the distance from the position of

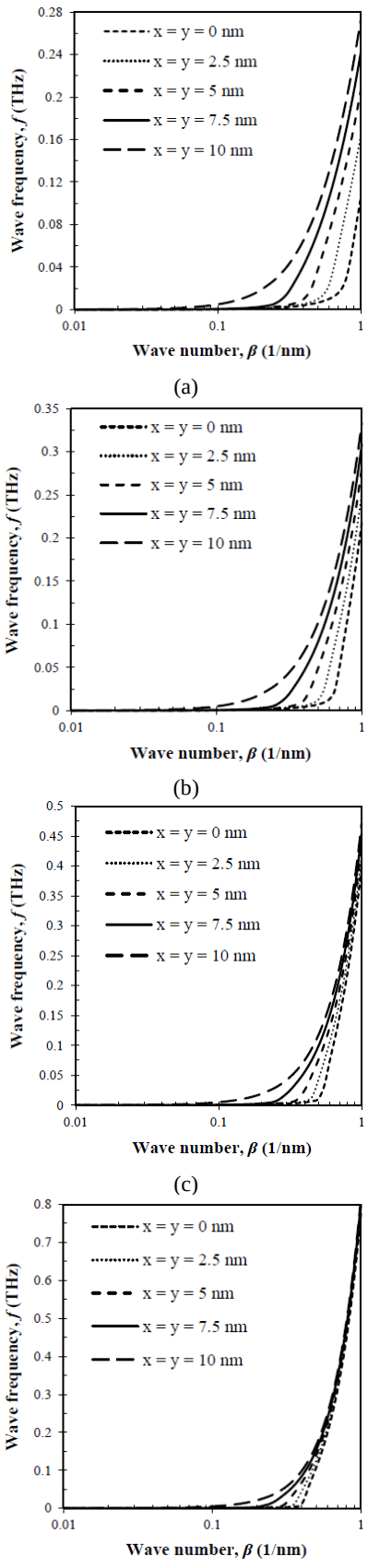

Fig. 3 The wave frequency variation against wave number for various x and y amounts at (a) η = 0 nm; (b) η = 0.5 nm; (c) η = 1 nm; (d) η = 2 nm (μ = 1 nm, $k_w = k_p = 0$, $\zeta = \lambda = 1$, N = 1)

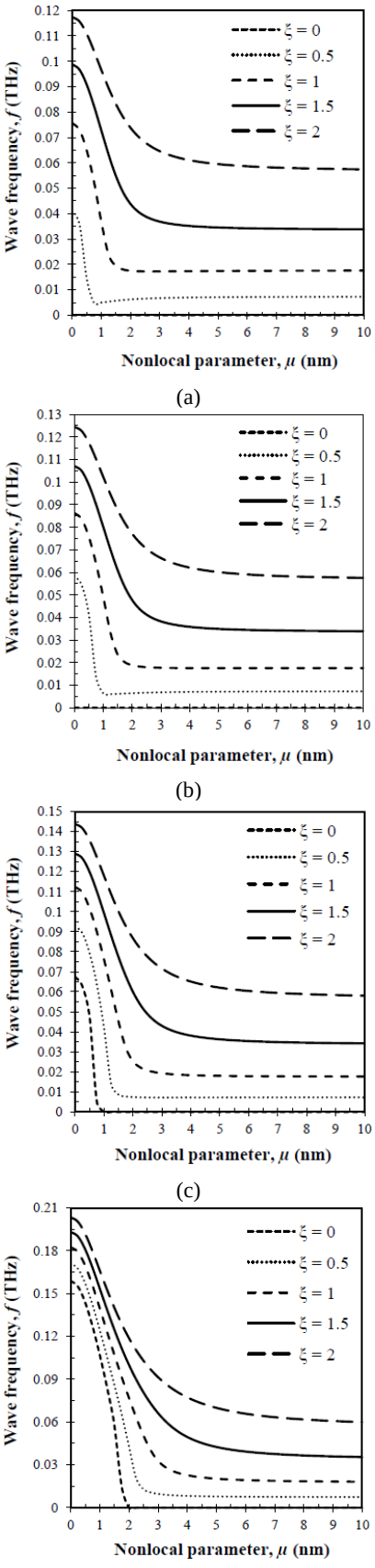

Fig. 4 The wave frequency variation against nonlocal parameter for various load factors at (a) η = 0 nm; (b) η = 0.5 nm; (c) η = 1 nm; (d) η = 2 nm (μ = 1 nm, $k_w = k_p = 0$, $\zeta = \lambda = 1$, N = 1)

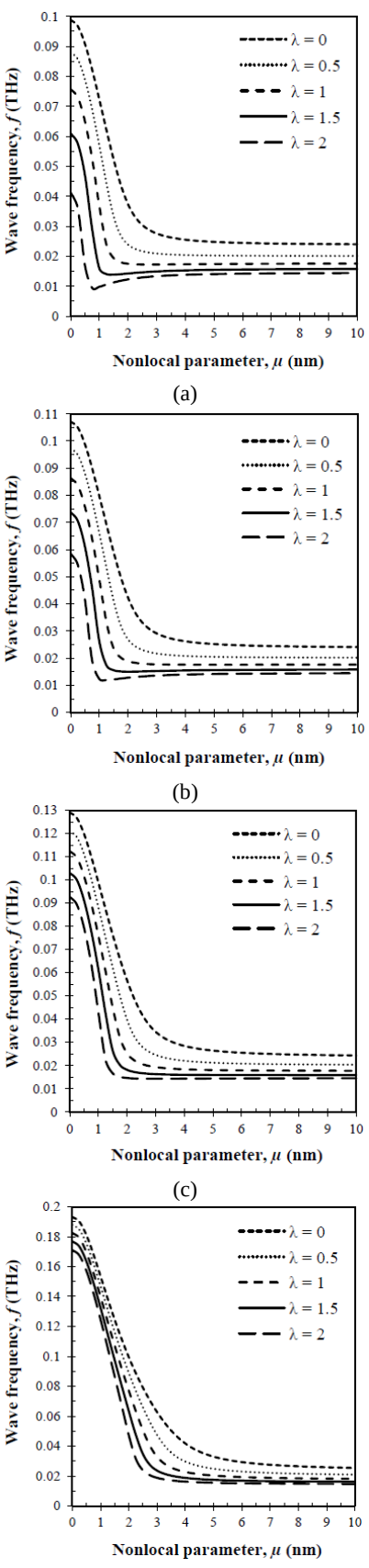

Fig. 5 The wave frequency variation against nonlocal parameter for different biaxial load factors at (a) η = 0 nm; (b) η = 0.5 nm; (c) η = 1 nm; (d) η = 2 nm (μ = 1 nm, $k_w = k_p = 0$, $\zeta = \lambda = 1$, N = 1)

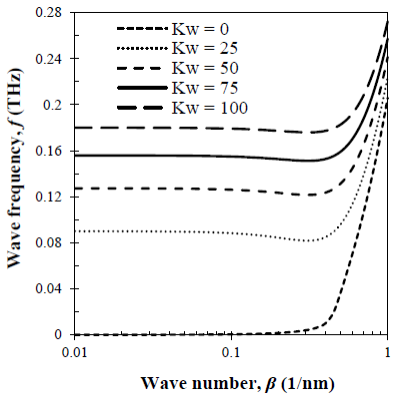

(a)

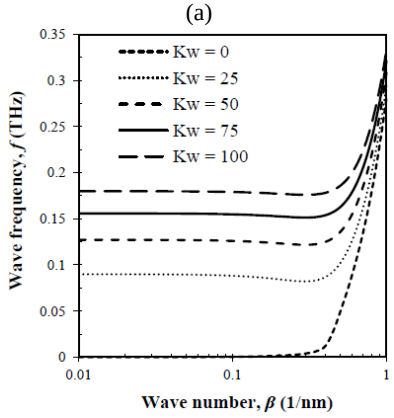

(b)

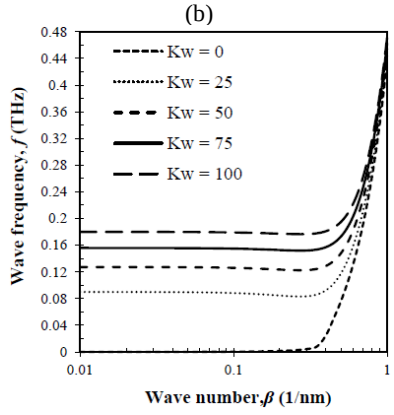

(c)

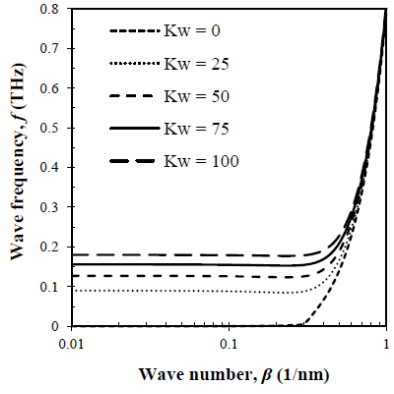

(d)

Fig. 6 The wave frequency variation against wave number for different Winkler coefficients at (a) η = 0 nm; (b) η = 0.5 nm; (c) η = 1 nm; (d) η = 2 nm (μ = 1 nm, $k_w = k_p = 0$, $\zeta = \lambda = 1$, N = 1)

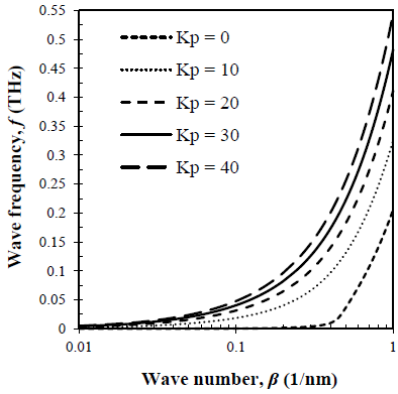

(a)

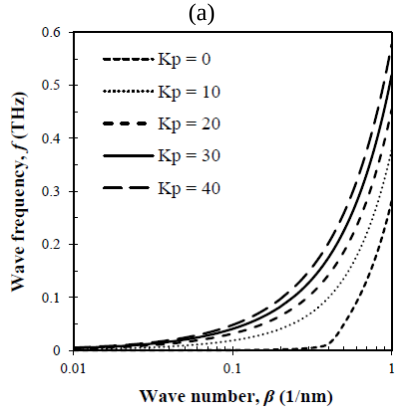

(b)

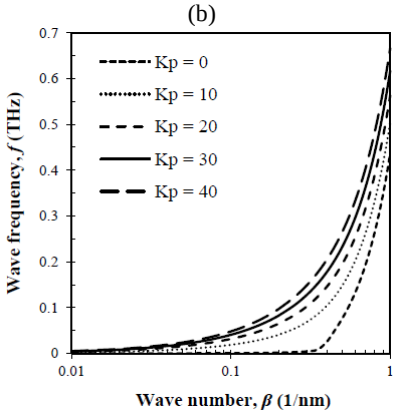

(c)

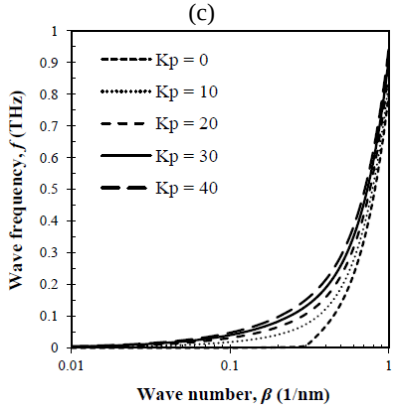

(d)

Fig. 7 The wave frequency variation against wave number for different Pasternak coefficients at (a) η = 0 nm; (b) η = 0.5 nm; (c) η = 1 nm; (d) η = 2 nm (μ = 1 nm, $k_w = k_p = 0$, $\zeta = \lambda = 1$, N = 1)

the place of loading to the origin of the GS, the higher wave frequencies are obtained. Therefore, it can be deduced that for achieving higher wave frequencies, the loading position shall be as far as possible from the origin. Moreover, the influences of different types of bending force, illustrated in Fig. 2 show that the small scale effects are covered as same as previous figure. Indeed, the load factor can be regarded as one of the increasing coefficients which are able to aggrandize wave frequency while it is increased. Obviously, in the first two conditions (a, b), the frequency values are all zero when nonlocality varies; however, in other situations (c, d), wave frequency is nonzero while nonlocality is smaller than 1 in Fig. 4(c) and 2 in Fig. 2(d). Further, the stiffness-softening effect can be seen here as well, which means reduction in the wave frequency is observed as the nonlocality rises. Further, it can also be noticed that the wave frequency remains constant after a particular amount of nonlocal parameter (μ > 7 nm). Influences of biaxial load factor are investigated in Fig. 5. In this diagram, the variations of wave frequency against nonlocal parameter are illustrated for different biaxial load factors.

As it is clear in this figure, the influences of biaxial load factor are completely different from the effects of load factor. In other words, increasing the load factor results in an increase in wave frequency, whereas, increasing biaxial load factor exhibits a reverse trend and have a detrimental effect on the wave frequency. Another difference is the nonzero amount of wave frequency for various values of biaxial load factor while wave frequency reaches to zero in some nonlocal parameters (at η = 0, η = 0.5). In contrast to the previous diagram, here, wave frequency does not vary once μ > 7 nm. Besides the discussed issues, influences of foundation parameters should be well studied. The effect of Winkler coefficient is illustrated in Fig. 6. This figure emphasizes that the size-dependency of the GS is similar to the former ones. The crucial point is that Winkler parameter can produce a raise in the amount of wave frequency whenever it is amplified. Meanwhile, it is significant to point that the mentioned coefficient can modify wave frequency in a particular range of wave numbers, roughly smaller than $\beta = 1 \times 10^9$ m.s. Finally, Fig. 7 is dedicated to clarify the influence of Pasternak coefficient on the wave frequency values. Herein, it is obvious that the wave frequency improves with the increasing Pasternak coefficient. However, the shape of the diagram is a bit different with the previous figure. Actually, by changing Winkler coefficient, the most observable changes can be seen in very small wave numbers. However, the most remarkable changes in this diagram can be observed in wave numbers between $\beta = 0.1 \times 10^9$ and $\beta = 1 \times 10^9$.

5. Conclusions

Since the behavior of SLGSs subjected to IVB force has not been scrutinized in the literature, this study investigates the WP responses of the mentioned structure while rested on elastic medium under described external loads. In this paper, it was attempted to employ the constitutive relations of the NSGT in order to capture both stiffness-softening and -hardening effects. In the framework of the Hamilton's Principle (HP), the nonlocal governing equations were derived and solved analytically. Then, wave frequencies were determined. The most important results can be summarized as follows:

• By increasing nonlocal parameter, wave frequency becomes smaller, whereas, mentioned variant can be grater if the length scale parameter is added.

• If each of the Winkler or Pasternak coefficients are added, wave frequency obtains higher amount.

• Higher wave frequencies are achieved whenever load factor is increased.

Higher wave frequencies are achieved whenever biaxial load factor is decreased.

References

Akbaş, Ş.D. (2018), "Bending of a cracked functionally graded nanobeam", *Adv. Nano Res., Int. J.*, **6**(3), 219-242. https://doi.org/10.12989/anr.2018.6.3.219.

Alabduljabbar, H., Haido, J.H., Alyousef, R., Yousif, S.T., McConnell, J., Wakil, K. and Jermsittiparsert, K. (2020), "Prediction of the flexural behavior of corroded concrete beams using combined method", *Structures*, **25**, 1000-1008. https://doi.org/10.1016/j.istruc.2020.03.057.

Alaskar, A., Alyousef, R., Alabduljabbar, H., Alrshoudi, F., Mohamed, A.M., Jermsittiparsert, K. and Ho, L.S. (2020a), "Elevated temperature resistance of concrete columns with axial loading", *Adv. Concrete Constr., Int. J.*, **9**(4), 355-365. https://doi.org/10.12989/acc.2020.9.4.355.

Alaskar, A., Shah, S.N.R., Keerio, M.A., Phulpoto, J.A., Baharom, S., Assilzadeh, H., Alyousef, R., Alabduljabbar, H. and Mohamed, A.M. (2020b), "Development of Pozzolanic material from clay", *Adv. Concrete Constr., Int. J.*, **10**(4), 301-310. https://doi.org/10.12989/acc.2020.10.4.301.

Alaskar, A., Wakil, K., Alyousef, R., Jermsittiparsert, K., Ho, L.S., Alabduljabbar, H., Alrshoudi, F. and Mohamed, A.M. (2020c), "Computational analysis of three dimensional steel frame structures through different stiffening members", *Steel Compos. Struct., Int. J.*, **35**(2), 187-197. https://doi.org/10.12989/scs.2020.35.2.187.

Alyousef, R., Alabduljabbar, H., Mohamed, A.M., Alaskar, A., Jermsittiparsert, K. and Ho, L.S. (2020), "A model to develop the porosity of concrete as important mechanical property", *Smart Struct. Syst., Int. J.*, **26**(2), 147-156. https://doi.org/10.12989/sss.2020.26.2.147.

Arani, A.G., Haghparast, E. and Zarei, H.B. (2016), "Nonlocal vibration of axially moving graphene sheet resting on orthotropic visco-Pasternak foundation under longitudinal magnetic field", *Physica B Condens. Matter*, **495**, 35-49. https://doi.org/10.1016/j.physb.2016.04.039.

Arash, B., Wang, Q. and Liew, K.M. (2012), "Wave propagation in graphene sheets with nonlocal elastic theory via finite element formulation", *Comput. Methods Appl. Mech. Eng.*, **223**, 1-9. https://doi.org/10.1016/j.cma.2012.02.002.

Aydogdu, M. (2009), "A general nonlocal beam theory: Its application to nanobeam bending, buckling and vibration", *Physica E Low Dimens. Syst. Nanostruct.*, **41**(9), 1651-1655. https://doi.org/10.1016/j.physe.2009.05.014.

Cai, C., Gao, X., Teng, Q., Kiran, R., Liu, J., Wei, Q. and Shi, Y. (2020a), "Hot isostatic pressing of a near α-ti alloy: Temperature optimization, microstructural evolution and mechanical performance evaluation", *Mater. Sci. Eng. A*, **2020**, 140426. https://doi.org/10.1016/j.msea.2020.140426.

Cai, C., Tey, W.S., Chen, J., Zhu, W., Liu, X., Liu, T., Zhao, L. and Zhou, K. (2020b), "Comparative study on 3D printing of polyamide 12 by selective laser sintering and multi jet fusion", *J. Mater. Process. Technol.*, **288**, 116882. https://doi.org/10.1016/j.jmatprotec.2020.116882.

Cai, C., Wu, X., Liu, W., Zhu, W., Chen, H., Qiu, J.C.D., Sun, C.N., Liu, J., Wei, Q. and Shi, Y. (2020c), "Selective laser melting of near-α titanium alloy Ti-6Al-2Zr-1Mo-1V: Parameter optimization, heat treatment and mechanical performance", *J. Mater. Process. Technol.*, **57**, 51-64. https://doi.org/10.1016/j.jmst.2020.05.004.

Cao, Y., Alyousef, R., Jermsittiparsert, K., Ho, L.S., Alaskar, A., Alabduljabbar, H., Alrshoudi, F. and Mohamed, A.M. (2020a), "Investigation on the monotonic behavior of the steel rack upright-beam column connection", *Smart Struct. Syst., Int. J.*, **26**(1), 103-115. https://doi.org/10.12989/sss.2020.26.1.103.

Cao, Y., Fan, Q., Azar, S.M., Alyousef, R., Yousif, S.T., Wakil, K., Jermsittiparsert, K., Ho, L.S., Alabduljabbar, H. and Alaskar, A. (2020b), "Computational parameter identification of strongest influence on the shear resistance of reinforced concrete beams by fiber reinforcement polymer", *Structures*, **27**, 118-127. https://doi.org/10.1016/j.istruc.2020.05.031.

Cao, Y., Wakil, K., Alyousef, R., Jermsittiparsert, K., Ho, L.S., Alabduljabbar, H., Alaskar, A., Alrshoudi, F. and Mohamed, A.M. (2020c), "Application of extreme learning machine in behavior of beam to column connections", *Structures*, **25**, 861-867. https://doi.org/10.1016/j.istruc.2020.03.058.

Cao, Y., Wakil, K., Alyousef, R., Yousif, S.T., Jermsittiparsert, K., Ho, L.S., Alabduljabbar, H., Alaskar, A., Alrshoudi, F. and Mohamed, A.M. (2020d), "Computational earthquake performance of plan-irregular shear wall structures subjected to different earthquake shock situations", *Earthq. Struct., Int. J.*, **18**(5), 567-580. https://doi.org/10.12989/eas.2020.18.5.567.

Chen, S., Hassanzadeh-Aghdam, M. and Ansari, R. (2018). "An analytical model for elastic modulus calculation of SiC whisker-reinforced hybrid metal matrix nanocomposite containing SiC nanoparticles", *J. Alloys Compd.*, **767**, 632-641. https://doi.org/10.1016/j.jallcom.2018.07.102.

Chen, C., Wang, X., Wang, Y., Yang, D., Yao, F., Zhang, W., Wang, B., Sewvandi, G.A., Yang, D. and Hu, D. (2020), "Additive manufacturing of piezoelectric materials", *Adv. Func. Mater.*, **30**(52), 2005141. https://doi.org/10.1002/adfm.202005141.

Ebrahimi, F. and Salari, E. (2015), "Thermo-mechanical vibration analysis of a single-walled carbon nanotube embedded in an elastic medium based on higher-order shear deformation beam theory", *J. Mech. Sci. Technol.*, **29**(9), 3797-3803. https://doi.org/10.1007/s12206-015-0826-2.

Ebrahimi, F. and Barati, M.R. (2016a), "Magneto-electro-elastic buckling analysis of nonlocal curved nanobeams", *Eur. Phys. J. Plus*, **131**(9), 346. https://doi.org/10.1140/epjp/i2016-16346-5.

Ebrahimi, F. and Barati, M.R. (2016b), "A nonlocal higher-order shear deformation beam theory for vibration analysis of size-dependent functionally graded nanobeams", *Arab. J. Sci. Eng.*, **41**(5), 1679-1690. https://doi.org/10.1007/s13369-015-1930-4.

Ebrahimi, F. and Barati, M.R. (2016c), "Static stability analysis of smart magneto-electro-elastic heterogeneous nanoplates embedded in an elastic medium based on a four-variable refined plate theory", *Smart Mater, Struct.*, **25**(10), 105014. https://doi.org/10.1088/0964-1726/25/10/105014.

Ebrahimi, F. and Barati, M.R. (2016d), "A unified formulation for dynamic analysis of nonlocal heterogeneous nanobeams in hygro-thermal environment", *Appl. Phys. A*, **122**(9), 792. https://doi.org/10.1007/s00339-016-0322-2.

Ebrahimi, F. and Barati, M.R. (2016e), "Vibration analysis of nonlocal beams made of functionally graded material in thermal environment", *Eur. Phys. J. Plus*, **131**(8), 279. https://doi.org/10.1140/epjp/i2016-16279-y.

Ebrahimi, F. and Hosseini, S. (2016), "Thermal effects on nonlinear vibration behavior of viscoelastic nanosize plates", *J. Therm. Stress.*, **39**(5), 606-625. https://doi.org/10.1080/01495739.2016.1160684.

Ebrahimi, F. and Barati, M.R. (2017a), "Buckling analysis of smart size-dependent higher order magneto-electro-thermo-elastic functionally graded nanosize beams", *J. Mech.*, **33**(1), 23-33. https://doi.org/10.1017/jmech.2016.46.

Ebrahimi, F. and Barati, M.R. (2017b), "Hygrothermal effects on vibration characteristics of viscoelastic FG nanobeams based on nonlocal strain gradient theory", *Compos. Struct.*, **159**, 433-444. https://doi.org/10.1016/j.compstruct.2016.09.092.

Ebrahimi, F. and Barati, M.R. (2017c), "Vibration analysis of viscoelastic inhomogeneous nanobeams incorporating surface and thermal effects", *Appl. Phys. A*, **123**(1), 5. https://doi.org/10.1007/s00339-016-0511-z.

Ebrahimi, F. and Dabbagh, A. (2017), "Wave propagation analysis of smart rotating porous heterogeneous piezo-electric nanobeams", *Eur. Phys. J. Plus*, **132**(4), 153. https://doi.org/10.1140/epjp/i2017-11366-3.

Ebrahimi, F. and Shafiei, N. (2017), "Influence of initial shear stress on the vibration behavior of single-layered graphene sheets embedded in an elastic medium based on Reddy's higher-order shear deformation plate theory", *Mech. Adv. Mater. Struct.*, **24**(9), 761-772. https://doi.org/10.1080/15376494.2016.1196781.

Ebrahimi, F. and Barati, M.R. (2018), "Effect of three-parameter viscoelastic medium on vibration behavior of temperature-dependent non-homogeneous viscoelastic nanobeams in a hygro-thermal environment", *Mech. Adv. Mater. Struct.*, **25**(5), 361-374. https://doi.org/10.1080/15376494.2016.1255831.

Ebrahimi, F., Barati, M.R. and Dabbagh, A. (2016a), "Wave dispersion characteristics of axially loaded magneto-electro-elastic nanobeams", *Appl. Phys. A*, **122**(11), 949. https://doi.org/10.1007/s00339-016-0465-1.

Ebrahimi, F., Barati, M.R. and Haghi, P. (2016b), "Nonlocal thermo-elastic wave propagation in temperature-dependent embedded small-scaled nonhomogeneous beams", *Eur. Phys. J. Plus*, **131**(11), 383. https://doi.org/10.1140/epjp/i2016-16383-0.

Ebrahimi, F., Dabbagh, A. and Barati, M.R. (2016c), "Wave propagation analysis of a size-dependent magneto-electro-elastic heterogeneous nanoplate", *Eur. Phys. J. Plus*, **131**(12), 1-18. https://doi.org/10.1140/epjp/i2016-16433-7.

Ebrahimi, F., Ghasemi, F. and Salari, E. (2016d), "Investigating thermal effects on vibration behavior of temperature-dependent compositionally graded Euler beams with porosities", *Meccanica*, **51**(1), 223-249. https://doi.org/10.1007/s11012-015-0208-y.

Eltaher, M., Alshorbagy, A.E. and Mahmoud, F. (2013), "Vibration analysis of Euler-Bernoulli nanobeams by using finite element method", *Appl. Math. Model.*, **37**(7), 4787-4797. https://doi.org/10.1016/j.apm.2012.10.016.

Farajpour, A., Yazdi, M.H., Rastgoo, A. and Mohammadi, M. (2016), "A higher-order nonlocal strain gradient plate model for buckling of orthotropic nanoplates in thermal environment", *Acta Mechanica*, **227**(7), 1849-1867. https://doi.org/10.1007/s00707-016-1605-6.

Gao, N. and Zhang, Y. (2019), "A low frequency underwater metastructure composed by helix metal and viscoelastic damping rubber", *J. Vib. Control*, **25**(3), 538-548. https://doi.org/10.1177/1077546318788446.

Gao, N., Hou, H. and Wu, J.H. (2018a), "A composite and deformable honeycomb acoustic metamaterial", *Int. J. Mod. Phys. B*, **32**(20), 1850204. https://doi.org/10.1142/S0217979218502041.

Gao, N., Hou, H., Zhang, Y. and Wu, J.H. (2018b), "Sound absorption of a new oblique-section acoustic metamaterial with

nested resonator", *Mod. Phys. Lett. B*, **32**(4), 1850040. https://doi.org/10.1142/S0217984918500409.

Ghadiri, M. and Shafiei, N. (2016), "Nonlinear bending vibration of a rotating nanobeam based on nonlocal Eringen's theory using differential quadrature method", *Microsyst. Technol.*, **22**(12), 2853-2867. https://doi.org/10.1007/s00542-015-2662-9.

Guo, H., Qian, K., Cai, A., Tang, J. and Liu, J. (2019), "Ordered gold nanoparticle arrays on the tip of silver wrinkled structures for single molecule detection", *Sens. Actuators B Chem.*, **300**, 126846. https://doi.org/10.1016/j.snb.2019.126846.

Guo, H., Li, X., Zhu, Q., Zhang, Z., Liu, Y., Li, Z., Wen, H., Li, Y., Tang, J. and Liu, J. (2020), "Imaging nano-defects of metal waveguides using the microwave cavity interference enhancement method", *Nanotechnology*, **31**(45), 455203. https://doi.org/10.1088/1361-6528/abaa74.

Hu, Y., Chen, Q., Feng, S. and Zuo, C. (2020), "Microscopic fringe projection profilometry: A review", *Opt. Lasers Eng.*, **135**,106192. https://doi.org/10.1016/j.optlaseng.2020.106192.

Huang, J., Alyousef, R., Meldi, S., Baharom, S., Alabduljabbar, H., Alaskar, A. and Assilzadeh, H. (2020a), "Influence of porosity and cement grade on concrete mechanical properties", *Adv. Concrete Constr., Int. J.*, **10**(5), 393-402. http://dx.doi.org/10.12989/acc.2020.10.5.393.

Huang, Z., Zheng, H., Guo, L. and Mo, D. (2020b), "Influence of the position of artificial boundary on computation accuracy of conjugated infinite element for a finite length cylindrical shell", *Acoust. Aust.*, **48**(2), 287-294. https://doi.org/10.1007/s40857-020-00175-5.

Katebi, J., Shoaei-parchin, M., Shariati, M., Trung, N.T. and Khorami, M. (2019), "Developed comparative analysis of metaheuristic optimization algorithms for optimal active control of structures", *Eng. Comput.*, **36**, 1539-1558. https://doi.org/10.1007/s00366-019-00780-7.

Kheroubi, B., Benzair, A., Tounsi, A. and Semmah, A. (2016), "A new refined nonlocal beam theory accounting for effect of thickness stretching in nanoscale beams", *Adv. Nano Res., Int. J.*, **4**(4), 251-264. https://doi.org/10.12989/anr.2016.4.4.251.

Lam, D.C., Yang, F., Chong, A., Wang, J. and Tong, P. (2003), "Experiments and theory in strain gradient elasticity", *J. Mech. Phys. Solids*, **51**(8), 1477-1508. https://doi.org/10.1016/S0022-5096(03)00053-X.

Lee, C., Wei, X., Kysar, J.W. and Hone, J. (2008), "Measurement of the elastic properties and intrinsic strength of monolayer graphene", *Science*, **321**(5887), 385-388. https://doi.org/10.1126/science.1157996.

Li, L. and Hu, Y. (2015), "Buckling analysis of size-dependent nonlinear beams based on a nonlocal strain gradient theory", *Int. J. Eng. Sci.*, **97**, 84-94. https://doi.org/10.1016/j.ijengsci.2015.08.013.

Li, L., Tang, H. and Hu, Y. (2018), "The effect of thickness on the mechanics of nanobeams", *Int. J. Eng. Sci.*, **123**, 81-91. https://doi.org/10.1016/j.ijengsci.2017.11.021.

Lim, C., Zhang, G. and Reddy, J. (2015), "A higher-order nonlocal elasticity and strain gradient theory and its applications in wave propagation", *J. Mech. Phys. Solids*, **78**, 298-313. https://doi.org/10.1016/j.jmps.2015.02.001.

Liu, C., Huang, X., Wu, Y.Y., Deng, X., Liu, J., Zheng, Z. and Hui, D. (2020a), "Review on the research progress of cement-based and geopolymer materials modified by graphene and graphene oxide", *Nanotechnol. Rev.*, **9**(1), 155-169. https://doi.org/10.1515/ntrev-2020-0014.

Liu, C., Wu, X., Wakil, K., Jermsittiparsert, K., Ho, L.S., Alabduljabbar, H., Alaskar, A., Alrshoudi, F., Alyousef, R. and Mohamed, A.M. (2020b), "Computational estimation of the earthquake response for fibre reinforced concrete rectangular columns", *Steel Compos. Struct., Int. J.*, **34**(5), 743-767. https://doi.org/10.12989/scs.2020.34.5.743.

Liu, H., Liu, X., Zhao, F., Liu, Y., Liu, L., Wang, L., Geng, C. and Huang, P. (2020c), "Preparation of a hydrophilic and antibacterial dual function ultrafiltration membrane with quaternized graphene oxide as a modifier", *J. Colloid Interface Sci.*, **562**, 182-192. https://doi.org/10.1016/j.jcis.2019.12.017.

Luo, L., Nguyen, H., Alabduljabbar, H., Alaskar, A., Alrshoudi, F., Alyousef, R., Nguyen, V.D. and Dang, H.M. (2020), "Depiction of concrete structures with seismic separation under faraway fault earthquakes", *Adv. Concrete Constr., Int. J.*, **9**(1), 71-82. https://doi.org/10.12989/acc.2020.9.1.071.

Malekzadeh, P., Setoodeh, A. and Beni, A.A. (2011), "Small scale effect on the free vibration of orthotropic arbitrary straight-sided quadrilateral nanoplates", *Compos. Struct.*, **93**(7), 1631-1639. https://doi.org/10.1016/j.compstruct.2011.01.008.

Mansouri, I., Shariati, M., Safa, M., Ibrahim, Z., Tahir, M. and Petković, D. (2019), "Analysis of influential factors for predicting the shear strength of a V-shaped angle shear connector in composite beams using an adaptive neuro-fuzzy technique", *J. Intell. Manuf.*, **30**(3), 1247-1257. https://doi.org/10.1007/s10845-017-1306-6.

Milovancevic, M., Marinović, J.S., Nikolić, J., Kitić, A., Shariati, M., Trung, N.T., Wakil, K. and Khorami, M. (2019), "UML diagrams for dynamical monitoring of rail vehicles", *Physica A*, **53**, 121169. https://doi.org/10.1016/j.physa.2019.121169.

Mohammadhassani, M., Nezamabadi-Pour, H., Suhatril, M. and Shariati, M. (2013), "Identification of a suitable ANN architecture in predicting strain in tie section of concrete deep beams", *Struct. Eng. Mech., Int. J.*, **46**(6), 853-868. https://doi.org/10.12989/sem.2013.46.6.853.

Mohammadhassani, M., Nezamabadi-Pour, H., Suhatril, M. and Shariati, M. (2014), "An evolutionary fuzzy modelling approach and comparison of different methods for shear strength prediction of high-strength concrete beams without stirrups", *Smart Struct. Syst., Int. J.*, **14**(5), 785-809. https://doi.org/10.12989/sss.2014.14.5.785.

Murmu, T. and Pradhan, S. (2009), "Vibration analysis of nano-single-layered graphene sheets embedded in elastic medium based on nonlocal elasticity theory", *J. Appl. Phys.*, **105**(6), 064319. https://doi.org/10.1063/1.3091292.

Murmu, T., McCarthy, M. and Adhikari, S. (2013), "In-plane magnetic field affected transverse vibration of embedded single-layer graphene sheets using equivalent nonlocal elasticity approach", *Compos. Struct.*, **96**, 57-63. https://doi.org/10.1016/j.compstruct.2012.09.005.

Narendar, S. and Gopalakrishnan, S. (2012), "Temperature effects on wave propagation in nanoplates", *Compos. Part B Eng.*, **43**(3), 1275-1281. https://doi.org/10.1016/j.compositesb.2011.11.029.

Natarajan, C.M., Tanner, M.G. and Hadfield, R.H. (2012), "Superconducting nanowire single-photon detectors: physics and applications", *Supercond. Sci. Technol.*, **25**(6), 063001. https://doi.org/10.1088/0953-2048/25/6/063001.

Phung-Van, P., Ferreira, A., Nguyen-Xuan, H. and Wahab, M.A. (2017a), "An isogeometric approach for size-dependent geometrically nonlinear transient analysis of functionally graded nanoplates", *Compos. Part B Eng.*, **118**, 125-134. https://doi.org/10.1016/j.compositesb.2017.03.012.

Phung-Van, P., Lieu, Q.X., Nguyen-Xuan, H. and Wahab, M.A. (2017b), "Size-dependent isogeometric analysis of functionally graded carbon nanotube-reinforced composite nanoplates", *Compos. Struct.*, **166**, 120-135. https://doi.org/10.1016/j.compstruct.2017.01.049.

Phung-Van, P., Thai, C.H., Nguyen-Xuan, H. and Abdel-Wahab, M. (2019a), "An isogeometric approach of static and free vibration analyses for porous FG nanoplates", *Eur. J. Mech. A Solids*, **78**, 103851. https://doi.org/10.1016/j.euromechsol.2019.103851.

Phung-Van, P., Thai, C.H., Nguyen-Xuan, H. and Wahab, M.A. (2019b), "Porosity-dependent nonlinear transient responses of functionally graded nanoplates using isogeometric analysis", *Compos. Part B Eng.*, **164**, 215-225. https://doi.org/10.1016/j.compositesb.2018.11.036.

Pradhan, S. and Murmu, T. (2010), "Small scale effect on the buckling analysis of single-layered graphene sheet embedded in an elastic medium based on nonlocal plate theory", *Physica E Low Dimens. Syst. Nanostruct.*, **42**(5), 1293-1301. https://doi.org/10.1016/j.physe.2009.10.053.

Pradhan, S. and Kumar, A. (2011), "Vibration analysis of orthotropic graphene sheets using nonlocal elasticity theory and differential quadrature method", *Compos. Struct.*, **93**(2), 774-779. https://doi.org/10.1016/j.compstruct.2010.08.004.

Qi, C.C. (2020), "Big data management in the mining industry", *Int. J. Miner. Metall. Mater.*, **27**(2), 131-139. https://doi.org/10.1007/s12613-019-1937-z.

Qian, J., Feng, S., Li, Y., Tao, T., Han, J., Chen, Q. and Zuo, C. (2020a), "Single-shot absolute 3D shape measurement with deep-learning-based color fringe projection profilometry", *Opt. Lett.*, **45**(7), 1842-1845. https://doi.org/10.1364/OL.388994.

Qian, J., Feng, S., Tao, T., Hu, Y., Li, Y., Chen, Q. and Zuo, C. (2020b), "Deep-learning-enabled geometric constraints and phase unwrapping for single-shot absolute 3D shape measurement", *APL Photonics*, **5**(4), 046105. https://doi.org/10.1063/5.0003217.

Qiu, T., Shi, X., Wang, J., Li, Y., Qu, S., Cheng, Q., Cui, T. and Sui, S. (2019), "Deep learning: A rapid and efficient route to automatic metasurface design", *Adv. Sci.*, **6**(12), 1900128. https://doi.org/10.1002/advs.201900128.

Rouhi, S. and Ansari, R. (2012), "Atomistic finite element model for axial buckling and vibration analysis of single-layered graphene sheets", *Physica E Low Dimens. Syst. Nanostruct.*, **44**(4), 764-772. https://doi.org/10.1016/j.physe.2011.11.020.

Sadeghipour Chahnasir, E., Zandi, Y., Shariati, M., Dehghani, E., Toghroli, A., Mohamed, E.T., Shariati, A., Safa, M., Wakil, K. and Khorami, M. (2018), "Application of support vector machine with firefly algorithm for investigation of the factors affecting the shear strength of angle shear connectors", *Smart Struct. Syst., Int. J.*, **22**(4), 413-424. http://dx.doi.org/10.12989/sss.2018.22.4.413.

Safa, M., Shariati, M., Ibrahim, Z., Toghroli, A., Baharom, S.B., Nor, N.M. and Petkovic, D. (2016), "Potential of adaptive neuro fuzzy inference system for evaluating the factors affecting steel-concrete composite beam's shear strength", *Steel Compos. Struct., Int. J.*, **21**(3), 679-688. http://dx.doi.org/10.12989/scs.2016.21.3.679.

Safa, M., Sari, P.A., Shariat, M., Suhatril, M., Trung, N.T., Wakil, K. and Khorami, M. (2020), "Development of neuro-fuzzy and neuro-bee predictive models for prediction of the safety factor of eco-protection slopes", *Physica A*, **550**, 124046. https://doi.org/10.1016/j.physa.2019.124046.

Sedghi, Y., Zandi, Y., Shariati, M., Ahmadi, E., Moghimi Azar, V., Toghroli, A., Safa, M., Tonnizam Mohamad, E., Khorami, M. and Wakil, K. (2018), "Application of ANFIS technique on performance of C and L shaped angle shear connectors", *Smart Struct. Syst., Int. J.*, **22**(3), 335-340. http://dx.doi.org/10.12989/sss.2018.22.3.335.

Seol, J.H., Jo, I., Moore, A.L., Lindsay, L., Aitken, Z.H., Pettes, M.T., Li, X., Yao, Z., Huang, R. and Broido, D. (2010), "Two-dimensional phonon transport in supported graphene", *Science*, **328**(5975), 213-216. https://doi.org/10.1126/science.1184014.

Shariati, A., Ebrahimi, F., Karimiasl, M., Vinyas, M. and Toghroli, A. (2020a), "On transient hygrothermal vibration of embedded viscoelastic flexoelectric/piezoelectric nanobeams under magnetic loading", *Adv. Nano Res., Int. J.*, **8**(1), 49-58. https://doi.org/10.12989/anr.2020.8.1.049.

Shariati, A., Hosseini, S.H.S., Bayrami, S.S., Ebrahimi, F. and Toghroli, A. (2020b), "Effect of residual surface stress on parametrically excited nonlinear dynamics and instability of viscoelastic piezoelectric nanoelectromechanical resonators", *Eng. Comput.*, **2020**, 1-16. https://doi.org/10.1007/s00366-019-00916-9.

Shi, M., Narayanasamy, M., Yang, C., Zhao, L., Jiang, J., Angaiah, S. and Yan, C. (2020a), "3D interpenetrating assembly of partially oxidized MXene confined Mn-Fe bimetallic oxide for superior energy storage in ionic liquid", *Electrochim. Acta*, **334**, 135546. https://doi.org/10.1016/j.electacta.2019.135546.

Shi, M., Xiao, P., Lang, J., Yan, C. and Yan, X. (2020b), "Porous g-C_3N_4 and MXene dual-confined FeOOH quantum dots for superior energy storage in an ionic liquid", *Adv. Sci.*, **7**(2), 1901975. https://doi.org/10.1002/advs.201901975.

Song, Q., Zhao, H., Jia, J., Yang, L., Lv, W., Gu, Q. and Shu, X. (2020), "Effects of demineralization on the surface morphology, microcrystalline and thermal transformation characteristics of coal", *J. Anal. Appl. Pyrolysis*, **145**, 104716. https://doi.org/10.1016/j.jaap.2019.104716.

Suhatril, M., Osman, N., Sari, P.A., Shariati, M. and Marto, A. (2019), "Significance of surface eco-protection techniques for cohesive soils slope in Selangor, Malaysia", *Geotech. Geol. Eng.*, **37**(3), 2007-2014. https://doi.org/10.1007/s10706-018-0740-3.

Tang, H., Li, L. and Hu, Y. (2019), "Coupling effect of thickness and shear deformation on size-dependent bending of micro/nano-scale porous beams", *Appl. Math. Model.*, **66**, 527-547. https://doi.org/10.1016/j.apm.2018.09.027.

Thai, C.H., Ferreira, A. and Phung-Van, P. (2019), "Size dependent free vibration analysis of multilayer functionally graded GPLRC microplates based on modified strain gradient theory", *Compos. Part B Eng.*, **169**, 174-188. https://doi.org/10.1016/j.compositesb.2019.02.048.

Thai, C.H., Ferreira, A., Tran, T. and Phung-Van, P. (2020), "A size-dependent quasi-3D isogeometric model for functionally graded graphene platelet-reinforced composite microplates based on the modified couple stress theory", *Compos. Struct.*, **234**, 111695. https://doi.org/10.1016/j.compstruct.2019.111695.

Toghroli, A., Mohammadhassani, M., Suhatril, M., Shariati, M. and Ibrahim, Z. (2014), "Prediction of shear capacity of channel shear connectors using the ANFIS model", *Steel Compos. Struct., Int. J.*, **17**(5), 623-639. http://dx.doi.org/10.12989/scs.2014.17.5.623.

Toghroli, A., Suhatril, M., Ibrahim, Z., Safa, M., Shariati, M. and Shamshirband, S. (2018), "Potential of soft computing approach for evaluating the factors affecting the capacity of steel-concrete composite beam", *J. Intell. Manuf.*, **29**(8), 1793-1801. https://doi.org/10.1007/s10845-016-1217-y.

Trung, N.T., Shahgoli, A.F., Zandi, Y., Shariati, M., Wakil, K., Safa, M. and Khorami, M. (2019), "Moment-rotation prediction of precast beam-to-column connections using extreme learning machine", *Struct. Eng. Mech., Int. J.*, **70**(5), 639-647. https://doi.org/10.12989/sem.2019.70.5.639.

Toghroli, A., Mehrabi, P., Shariati, M., Trung, N.T., Jahandari, S. and Rasekh, H. (2020), "Evaluating the use of recycled concrete aggregate and pozzolanic additives in fiber-reinforced pervious concrete with industrial and recycled fibers", *Constr. Build. Mater.*, **252**, 118997. https://doi.org/10.1016/j.conbuildmat.2020.118997.

Wang, Y.Z., Li, F.M. and Kishimoto, K. (2010), "Scale effects on the longitudinal wave propagation in nanoplates", *Physica E Low Dimens. Syst. Nanostruct.*, **42**(5), 1356-1360. https://doi.org/10.1016/j.physe.2009.11.036.

Wang, Y., Yao, M., Ma, R., Yuan, Q., Yang, D., Cui, B., Ma, C., Liu, M. and Hu, D. (2020), "Design strategy of barium titanate/polyvinylidene fluoride-based nanocomposite films for

high energy storage", *J. Mater. Chem. A*, **8**(3), 884-917. https://doi.org/10.1039/C9TA11527G.

Xiao, W., Li, L. and Wang, M. (2017), "Propagation of in-plane wave in viscoelastic monolayer graphene via nonlocal strain gradient theory", *Appl. Phys. A*, **123**(6), 388. https://doi.org/10.1007/s00339-017-1007-1.

Xu, Q., Zou, Z., Chen, Y., Wang, K., Du, Z., Feng, J., Ding, C., Bai, Z., Zang, Y. and Xiong, Y. (2020), "Performance of a novel-type of heat flue in a coke oven based on high-temperature and low-oxygen diffusion combustion technology", *Fuel*, **267**, 117160. https://doi.org/10.1016/j.fuel.2020.117160.

Yan, H., Xue, X., Chen, W., Wu, X., Dong, J., Liu, Y. and Wang, Z. (2020), "Reversible Na^+ insertion/extraction in conductive polypyrrole-decorated $NaTi_2$ (PO_4) 3 nanocomposite with outstanding electrochemical property", *Appl. Surf. Sci.*, **530**, 147295. https://doi.org/10.1016/j.apsusc.2020.147295.

Zenkour, A.M. (2016), "Nonlocal transient thermal analysis of a single-layered graphene sheet embedded in viscoelastic medium", *Physica Low Dimens. Syst. Nanostruct.*, **79**, 87-97. https://doi.org/10.1016/j.physe.2015.12.003.

Zhang, J., Chen, Q., Sun, J., Tian, L. and Zuo, C. (2020a), "On a universal solution to the transport-of-intensity equation", *Opt. Lett.*, **45**(13), 3649-3652. https://doi.org/10.1364/OL.391823.

Zhang, J., Sun, J., Chen, Q. and Zuo, C. (2020b), "Resolution analysis in a lens-free on-chip digital holographic microscope", *IEEE Trans. Comput. Imaging*, **6**, 697-710. https://doi.org/10.1109/TCI.2020.2964247.

Zhao, X., Fourie, A. and Qi, C.C. (2019), "An analytical solution for evaluating the safety of an exposed face in a paste backfill stope incorporating the arching phenomenon", *Int. J. Miner. Metall. Mater.*, **26**(10), 1206-1216. https://doi.org/10.1007/s12613-019-1885-7.

Zhao, X., Fourie, A. and Qi, C.C. (2020a), "Mechanics and safety issues in tailing-based backfill: A review", *Int. J. Miner. Metall. Mater.*, **27**(9), 1165-1178. https://doi.org/10.1007/s12613-020-2004-5.

Zhao, X., Fourie, A., Veenstra, R. and Qi, C.C. (2020b), "Safety of barricades in cemented paste-backfilled stopes", *Int. J. Miner. Metall. Mater.*, **27**(8), 1054-1064. https://doi.org/10.1007/s12613-020-2006-3.

Zhu, X. and Li, L. (2017a), "Closed form solution for a nonlocal strain gradient rod in tension", *Int. J. Eng. Sci.*, **119**, 16-28. ttps://doi.org/10.1016/j.ijengsci.2017.06.019.

Zhu, X. and Li, L. (2017b), "On longitudinal dynamics of nanorods", *Int. J. Eng. Sci.*, **120**, 129-145. https://doi.org/10.1016/j.ijengsci.2017.08.003.

Zhu, X. and Li, L. (2017c), "Twisting statics of functionally graded nanotubes using Eringen's nonlocal integral model", *Compos. Struct.*, **178**, 87-96. https://doi.org/10.1016/j.compstruct.2017.06.067.

Zhu, J., Wu, P., Chen, M., Kim, M.J., Wang, X. and Fang, T. (2020), "Automatically processing IFC clipping representation for BIM and GIS integration at the process level", *Appl. Sci.*, **10**(6), 2009. https://doi.org/10.3390/app10062009.

Zuo, C., Chen, Q., Gu, G., Feng, S., Feng, F., Li, R. and Shen, G. (2013), "High-speed three-dimensional shape measurement for dynamic scenes using bi-frequency tripolar pulse-width-modulation fringe projection", *Opt. Lasers Eng.*, **51**(8), 953-960. https://doi.org/10.1016/j.optlaseng.2013.02.012.

Zuo, C., Chen, Q., Tian, L., Waller, L. and Asundi, A. (2015), "Transport of intensity phase retrieval and computational imaging for partially coherent fields: The phase space perspective", *Opt. Lasers Eng.*, **71**, 20-32. https://doi.org/10.1016/j.optlaseng.2015.03.006.

Zuo, C., Sun, J., Li, J., Zhang, J., Asundi, A. and Chen, Q. (2017), "High-resolution transport-of-intensity quantitative phase microscopy with annular illumination", *Sci. Rep.*, **7**(1), 1-22. https://doi.org/10.1038/s41598-017-06837-1.

Zuo, C., Li, J., Sun, J., Fan, Y., Zhang, J., Lu, L., Zhang, R., Wang, B., Huang, L. and Chen, Q. (2020a), "Transport of intensity equation: A tutorial", *Opt. Lasers Eng.*, **135**, 106187. https://doi.org/10.1016/j.optlaseng.2020.106187.

Zuo, C., Sun, J., Li, J., Asundi, A. and Chen, Q. (2020b), "Wide-field high-resolution 3d microscopy with Fourier ptychographic diffraction tomography", *Opt. Lasers Eng.*, **128**, 106003. https://doi.org/10.1016/j.optlaseng.2020.106003.

CC

Appendix

$$\begin{cases} k_{11} = -\left(1+\eta^2\left(\frac{\partial^2}{\partial x^2}+\frac{\partial^2}{\partial y^2}\right)\right)\left(D_{11}{\beta_1}^4 + 2(D_{12}+2D_{66}){\beta_1}^2{\beta_2}^2 + D_{22}{\beta_2}^4\right) \\ +\left(1+\mu^2\left(\frac{\partial^2}{\partial x^2}+\frac{\partial^2}{\partial y^2}\right)\right)\left(k_p\left({\beta_1}^2+{\beta_2}^2\right) - k_w + N_x^0{\beta_1}^2 + N_y^0{\beta_2}^2\right) \\ k_{12} = -\left(1+\eta^2\left(\frac{\partial^2}{\partial x^2}+\frac{\partial^2}{\partial y^2}\right)\right)\left(D_{11}^s{\beta_1}^4 + 2(D_{12}^s+2D_{66}^s){\beta_1}^2{\beta_2}^2 + D_{22}^s{\beta_2}^4\right) \\ +\left(1+\mu^2\left(\frac{\partial^2}{\partial x^2}+\frac{\partial^2}{\partial y^2}\right)\right)\left(k_p\left({\beta_1}^2+{\beta_2}^2\right) - k_w + N_x^0{\beta_1}^2 + N_y^0{\beta_2}^2\right) \\ k_{21} = -\left(1+\eta^2\left(\frac{\partial^2}{\partial x^2}+\frac{\partial^2}{\partial y^2}\right)\right)\left(D_{11}^s{\beta_1}^4 + 2(D_{12}^s+2D_{66}^s){\beta_1}^2{\beta_2}^2 + D_{22}^s{\beta_2}^4\right) \\ +\left(1+\mu^2\left(\frac{\partial^2}{\partial x^2}+\frac{\partial^2}{\partial y^2}\right)\right)\left(k_p\left({\beta_1}^2+{\beta_2}^2\right) - k_w + N_x^0{\beta_1}^2 + N_y^0{\beta_2}^2\right) \\ k_{22} = -\left(1+\eta^2\left(\frac{\partial^2}{\partial x^2}+\frac{\partial^2}{\partial y^2}\right)\right)\left(\begin{matrix} H_{11}^s{\beta_1}^4 + 2(H_{12}^s+2H_{66}^s){\beta_1}^2{\beta_2}^2 + H_{22}^s{\beta_2}^4 \\ +A_{55}^s{\beta_1}^2 + A_{44}^s{\beta_2}^2 \end{matrix}\right) \\ +\left(1+\mu^2\left(\frac{\partial^2}{\partial x^2}+\frac{\partial^2}{\partial y^2}\right)\right)\left(k_p\left({\beta_1}^2+{\beta_2}^2\right) - k_w + N_x^0{\beta_1}^2 + N_y^0{\beta_2}^2\right) \end{cases} \tag{A1}$$

$$\begin{cases} m_{11} = -\left(1+\mu^2\left({\beta_1}^2+{\beta_2}^2\right)\right)\left(I_0 + I_2\left({\beta_1}^2+{\beta_2}^2\right)\right) \\ m_{12} = -\left(1+\mu^2\left({\beta_1}^2+{\beta_2}^2\right)\right)\left(I_0 + J_2\left({\beta_1}^2+{\beta_2}^2\right)\right) \\ m_{21} = -\left(1+\mu^2\left({\beta_1}^2+{\beta_2}^2\right)\right)\left(I_0 + J_2\left({\beta_1}^2+{\beta_2}^2\right)\right) \\ m_{22} = -\left(1+\mu^2\left({\beta_1}^2+{\beta_2}^2\right)\right)\left(I_0 + K_2\left({\beta_1}^2+{\beta_2}^2\right)\right) \end{cases} \tag{A2}$$